

3D Shape Knowledge Graph for Cross-domain 3D Shape Retrieval

Rihao Chang, Yongtao Ma, Tong Hao*, Weizhi Nie

Abstract—The surge in 3D modeling has led to a pronounced research emphasis on the field of 3D shape retrieval. Numerous contemporary approaches have been put forth to tackle this intricate challenge. Nevertheless, effectively addressing the intricacies of cross-modal 3D shape retrieval remains a formidable undertaking, owing to inherent modality-based disparities. This study presents an innovative notion—termed “geometric words”—which functions as elemental constituents for representing entities through combinations. To establish the knowledge graph, we employ geometric words as nodes, connecting them via shape categories and geometry attributes. Subsequently, we devise a unique graph embedding method for knowledge acquisition. Finally, an effective similarity measure is introduced for retrieval purposes. Importantly, each 3D or 2D entity can anchor its geometric terms within the knowledge graph, thereby serving as a link between cross-domain data. As a result, our approach facilitates multiple cross-domain 3D shape retrieval tasks. We evaluate the proposed method’s performance on the ModelNet40 and ShapeNetCore55 datasets, encompassing scenarios related to 3D shape retrieval and cross-domain retrieval. Furthermore, we employ the established cross-modal dataset (MI3DOR) to assess cross-modal 3D shape retrieval. The resulting experimental outcomes, in conjunction with comparisons against state-of-the-art techniques, clearly highlight the superiority of our approach.

Index Terms—3D shape retrieval, cross-domain 3D shape retrieval, cross-modal 3D shape retrieval, 3D shape knowledge graph.

I. INTRODUCTION

The advancement of digitalization methods and computer vision has led to the widespread utilization of 3D shapes in various domains such as computer-aided design, medical diagnostics, bioinformatics, 3D printing, medical imaging, and digital entertainment. In recent years, there has been a desire for quick generation and simple access to vast quantities of 3D shapes, particularly for applications in virtual and augmented reality. It is reasonable to utilize some references to obtain similar 3D shapes and accelerate secondary development. These references can be 3D shapes [1, 2], 2D images [3], sketch images [4], and text information [5]. Numerous methods have been put out in recent years to deal with this issue.

The MVCNN[3] extracts a series of rendered views on 2D pictures and combines information from several perspectives of a 3D shape into a single, compact shape descriptor.

Yongtao Ma and Rihao Chang are with the School of Microelectronics, Tianjin University, Tianjin 300072, China. (email: mayongtao@tju.edu.cn, changrihao@tju.edu.cn)

Weizhi Nie is with the School of Electrical and Information Engineering, Tianjin University, Tianjin 300072, China. (e-mail: weizhinie@tju.edu.cn)

*Corresponding author: Tong Hao is with the School of Life Sciences, Tianjin Normal University, Tianjin 300387, China.(e-mail: joyht2001@163.com)

PointNet++[6] iteratively implements the representations in a hierarchical neural network using point cloud representations for the input data to create a representation of three-dimensional forms. A multiloop-view convolutional neural network architecture for 3D shape retrieval was suggested by Gao et al.[7]. It may be seen of as a modified MVCNN that takes into account the natural hierarchical links between views. Some researchers, however, concentrate more on the multimodal information to effectively represent the 3D shapes. You et al.[8] suggested a combined convolutional network that successfully integrates point cloud and multiview images into an end-to-end neural network. These conventional methods concentrate on the descriptive layout of 3D shapes and use them to find related 3D shapes. However, consumers may now quickly obtain photographs thanks to the advancement of computer vision and smartphones. Some academics concentrate on the issue of retrieving cross-modal 3D shapes from 2D photos. Dai et al.[9] recommended a unique deep correlated holistic metric learning (DCHML) strategy to lessen the distinction between sketch images and 3D shapes. DCHML simultaneously trains modality-specific networks, mapping input data into an integrated feature space. Joint distribution adaptation (JDA), another transfer learning strategy, was put out by Long et al.[10]. It jointly adjusts the conditional distribution and the marginal distribution as part of a principled dimensionality reduction strategy to provide the effectiveness and robustness to significant distributional variations during feature learning. A coherent structure that minimizes the transition across domains statistically and geometrically has been proposed by Zhang et al.[11]. In order to simultaneously decrease the geometric shift and the propagation shift, two combined projections are trained that project the information from the source domain and the target domain into low-dimensional subspaces. All of these techniques, however, concentrate on cross-modal feature learning and global structural information descriptor creation. Both of these depend on parameter learning, extensive training datasets, and model design. All of these techniques have trouble retrieving several cross-domain 3D models at once. These techniques cannot thus be seen as union methods.

A. Motivation

Traditional 3D shape retrieval techniques suffer from three distinct issues:1) They heavily rely on extensive 3D shape datasets to train network parameters. 2) They are ill-suited for addressing cross-domain and cross-modal retrieval challenges, where the efficacy of one modality diminishes when applied to different datasets. 3) None of these methods can effectively

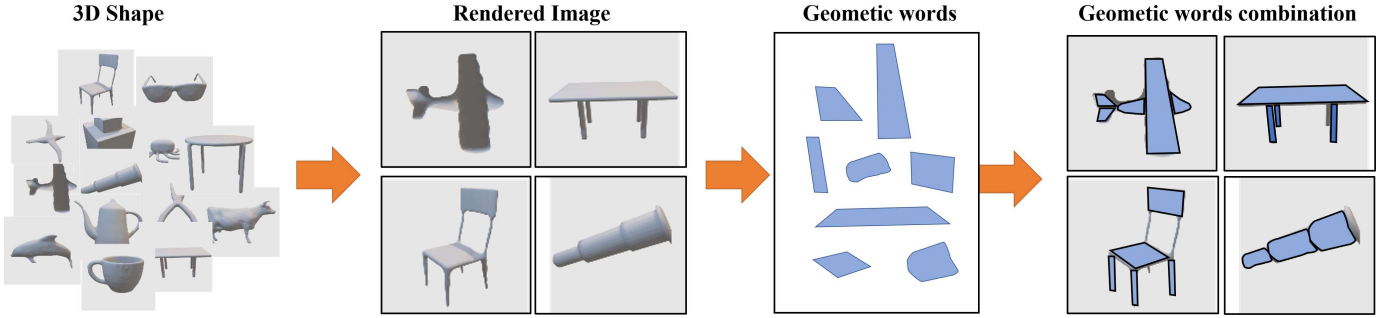


Fig. 1. The schematic diagram for inspiration. Each 3D shape can be represented by a set of 2D views. The 2D image can also be split into a set of part shapes. Finally, these part shapes can be mapped into a standard geometric shape. This means that any 3D shape or a 2D image can be represented by finite geometric shapes if we have a complete dictionary of geometric shapes. Based on this assumption, we can handle the traditional 3D shape retrieval problem, 2D image-based 3D shape retrieval problem and cross-domain 3D shape retrieval problem according to the geometric dictionary.

handle multi-condition cross-domain 3D model retrieval. This paper introduces a novel concept to bridge these gaps. By identifying an intermediary variable capable of representing both 2D images and 3D shape information, we can establish connections between diverse domains and modalities. This intermediary variable serves as a representation of shape information and facilitates guided feature learning. Thus, the task at hand is to determine how to identify and utilize this intermediary variable.

This paper introduces a novel concept to bridge these gaps. By identifying an intermediary variable capable of representing both 2D images and 3D shape information, we can establish connections between diverse domains and modalities. This intermediary variable serves as a representation of shape information and facilitates guided feature learning. Thus, the task at hand is to determine how to identify and utilize this intermediary variable.

In this paper, a novel idea is presented. If we can find an intermediate variable, which can be used to represent the 2D image and the 3D shape information, we will be able to bridge the gap between different domains and different modalities. Naturally, this variable can be used to represent the shape information and help to guide feature learning. Thus, we need to think about how to find this intermediate variable.

In Fig.1, a single 3D shape finds representation through a set of rendered images. Additionally, these rendered images can be deconstructed into a set containing geometric information. For example, a "cup" can be reduced to a cylinder, and a "table" can be decomposed into a square plane and a cylinder. When we treat a 3D shape as a document, its rendered images can be likened to sentences, while geometric information constitutes the "geometric words." These "geometric words" represent elemental shape components, allowing any shape to be expressed through a limitless combination of such words. Importantly, the term "geometric word" surpasses the conventional interpretation of geometric primitives, which encompasses standard shapes like cylinders, squares, and triangles. Instead, the concept of a "geometric word" boasts a broader scope, applicable to any shape. This perspective liberates us from relying on an extensive array of 3D shapes for training, as we can sufficiently describe shapes by generating an ample assortment of geometric words. This technique has the

potential to address cross-domain retrieval concerns, as each 3D shape can be delineated by an infinite array of geometric words. Furthermore, geometric information can be extracted from 2D images, bridging the gap between 2D images and 3D shapes and thus facilitating cross-modal 3D shape retrieval. Nonetheless, we are confronted with two pivotal challenges: 1) Defining and identifying the comprehensive set of "geometric words" serving as a holistic shape representation. 2) Devising methods for shape retrieval and cross-domain shape retrieval predicated upon these "geometric words."

This paper, grounded in the notion of "geometric words," proposes an innovative 3D shape knowledge graph and graph embedding technique to address the complexities of cross-domain 3D shape retrieval. We begin by leveraging OpenGL to construct a toolbox¹ for generating a set of rendered 3D shape images. Subsequently, we deploy an image segmentation approach to extract part shapes. The unsupervised technique of K-means is then employed to identify geometric words based on these part shapes. At this juncture, we have acquired a collection of rendered images and associated part shapes. The subsequent steps encompass the construction of a 3D shape knowledge graph that encapsulates the relationships among 3D shapes, rendered images, part shapes, and geometric words. A unique graph embedding strategy is subsequently introduced to facilitate the learning of embeddings for 3D shapes, rendered images, shape parts, and geometric words, incorporating their inherent structural attributes. Finally, an effective similarity measurement methodology is proposed to address 3D shape retrieval. Notably, our approach adeptly addresses cross-domain and cross-modal 3D shape retrieval in one unified framework, all the while requiring minimal data to establish the 3D shape knowledge network.

B. Contributions

The contributions of this paper are outlined as follows:

- We present a pioneering 3D shape knowledge graph that proficiently tackles the intricate challenges of cross-domain 3D shape retrieval. To the best of our knowledge, this study marks the inaugural application of the knowl-

¹Removed for anonymized peer review

edge graph paradigm to the realm of 3D shape retrieval, uniquely addressing multiple cross-domain aspects.

- A novel graph embedding strategy is proposed for representing entities within the 3D shape knowledge graph. This strategy effectively addresses representation learning under both supervised and unsupervised conditions.
- A similarity metric between query shapes/images and target 3D shapes, rooted in knowledge graph embeddings, is introduced. This metric adeptly incorporates geometric structural and categorical information of 3D shapes, resulting in enhanced retrieval precision.

The subsequent sections delineate the remaining content of this document. Section 2 expounds upon related work, while Section 3 introduces our proposed solution. Section 4 showcases experimental outcomes, elucidating the effectiveness of our approach. A comprehensive review of the results is also furnished in this section, employing our approach to confront a range of 3D shape retrieval challenges and demonstrate its efficacy. Lastly, Section 5 delves into potential avenues for future research.

II. RELATED WORK

In recent years, there has been a surge in the development of diverse 3D shape recognition methods. This section introduces classic 3D shape retrieval methods and recent advancements in cross-domain 3D shape retrieval.

A. 3D Shape Retrieval

The advancement of 3D data processing technology has led to the application of 3D shape retrieval across various domains. To convolve a 3D shape akin to any other tensor [12, 13], several studies have concentrated on voxelized shapes. These techniques encounter resolution constraints due to data sparseness and the computational expense associated with 3D convolution.

For the purpose of 3D object identification and retrieval, Garro et al. [14] introduced tree-based shape representations grounded in specific graph kernels and the scale space of the autodiffusion function (ADF), enabling the incorporation of texture and other structural information. Xie et al. [15], by estimating multiscale shape distributions and applying Fisher discriminant criteria to neurons, proposed a discriminative deep autoencoder for learning deformation-invariant shape information. PointNet [6] pioneered a technique for direct processing of point clouds using deep neural networks, albeit disregarding local features. These methodologies exhibit commendable performance on certain publicly available 3D shape datasets. Nevertheless, these approaches primarily rely on mathematical models to derive effective structural representations, neglecting geometric information of practical significance.

In the context of addressing classification and retrieval challenges, Wang et al. [16] introduced the EdgeConv module, suitable for point cloud tasks integrated with CNNs. Concurrently, other strategies tackle 3D representation using multiview data. The lighting field descriptor (LFD) [17] serves as an initial viewpoint-based 3D representation, comparing

the corresponding 2D properties of two view sets to ascertain the similarity between 3D objects. Similarly, GIFT [18] calculates the Hausdorff distance between their corresponding view sets. Traditional methods of 3D shape representation can be regarded as variants of LFD and GIFT. Su et al. [3] recently introduced a multi-view convolutional neural network (MVCNN), which generates numerous 2D projection features through CNN-based learning in a trainable end-to-end manner. Sfikas [19] proposed a technique for capturing panorama view features, aiming to ensure 3D shape continuity and minimize data preprocessing by creating an augmented image representation.

In recent years, graph structures have gained prominence in handling the representation of 3D models. Utilizing a graph neural network, Wang et al. [20] introduced local spectral graph convolution to jointly consider point information and information from neighboring points. Te et al. [21] employed spectral graph theory to develop a regularized graph convolutional neural network. This network maps the point cloud onto a graph structure and performs calculations on this structure using Chebyshev polynomial approximation.

To address classification and retrieval challenges, Wang et al. [16] proposed EdgeConv, an approach suitable for point cloud tasks within a CNN framework. Shi et al. [22] devised Point-GNN to mitigate translation variance and introduced a process of box merging and scoring to accurately aggregate detections from various vertices. Zhang et al. [23] introduced an edge-oriented graph convolutional network that leverages multidimensional edge information for relationship modeling and the study of interactions between nodes and edges. These methodologies emphasize the utilization of structural information to enhance the performance of 3D shape features. However, these graph-based approaches tend to overlook cross-modal relation information and local details of 3D shapes.

Both of these methods have developed corresponding networks for learning 3D form representations using prevalent deep learning techniques. These approaches rely extensively on abundant training data, rather than geometric structural data. Adapting these methodologies to address the challenge of cross-domain 3D shape retrieval presents a formidable task.

B. Cross-domain 3D Shape Retrieval

Cross-domain refers to the exploration that enable effective knowledge transfer [24, 25] and generalization between different, often unrelated, modalities or data sources [26], facilitating improved performance and insights across various tasks. Image-based retrieval has emerged as a contemporary technique with the potential to become a formidable competitor [27–29]. Mu et al. introduced a novel paradigm for image-based 3D shape recovery [30]. The approach initially represents the image as a Euclidean point, transforming all displayed views of a 3D shape into Symmetric Positive Definite (SPD) matrices, effectively representing them as points on a Riemannian manifold. The recovery of image-based 3D shape is then simplified into a process of learning Riemannian metrics from Euclidean metrics. Li et al. constructed an embedding space using a 3D shape similarity measure [31]. They

further employed a Convolutional Neural Network (CNN) to enhance the purity of images by eliminating distracting elements. This joint embedding strategy enables cross-view image retrieval, image-based shape retrieval, and shape-based image retrieval. Despite the limited availability of relevant works in the image retrieval community, these techniques have been established and serve as important references. Incorporating a Generative Adversarial Network (GAN) into the process, random noise drawn from a fixed distribution can be harnessed to generate coherent images while handling function transformations. The forthcoming sections provide detailed explanations of these methodologies. It is noteworthy to consider the definition of SeqViews2Seqlabels [32] during the feature extraction phase. To capture the global characteristics of 3D shapes, the SeqViews2Seqlabels model is introduced. This model maintains spatial and content knowledge across sequence views through aggregated sequences. Simultaneously, by adjusting the weight of specific views, the discriminative capacity of the SeqViews2Seqlabels model is enhanced. Upon closer examination, these approaches collectively constitute cross-domain feature learning. Their primary objective is to facilitate feature learning from multi-modal data within an embedding space. Notably, these approaches tend to overlook geometric information of practical significance.

C. 3D Model based on Component Theory

In this paper, we introduce a "geometric word" theory inspired by previous research [33], which serves as a versatile framework for representing shape information. Conceptually, a "geometric word" can be conceived as a fundamental constituent of an object, akin to the notion of components introduced in prior work on component theory. Liu et al. [34] presented an innovative formulation that encompasses the learning of physical primitives to expound both an object's visual attributes and its behavior within physical events. Their approach offers a compelling strategy for tackling segmentation challenges, particularly in the context of tool behaviors, while remaining adaptable to more traditional models. Katageri et al. [35] proposed the Point Decomposition Network (PointDCCNet) tailored for 3D object classification. This method relies critically on the performance of its decomposition module. Our methods are further inspired by certain multi-view 3D model segmentation strategies, such as those outlined in [36–38]. These approaches transform 3D point clouds into 2D images, effectively translating the 3D analysis into a 2D problem addressable through CNN-based solutions. Feng et al. [39] introduced the Group-view Convolutional Neural Network (GVCNN) as a means of hierarchical correlation modeling aimed at delivering discriminative 3D shape descriptions. By providing multiview information through a grouping mechanism, each group can be interpreted as a distinctive component. This design effectively eliminates redundant information, ultimately enhancing the final performance. Mo et al. [40] introduced an extensive 3D object dataset featuring intricate annotations and structured object parts. This dataset offers a valuable lens through which to comprehend 3D models and served as an inspiration for our

formulation of the geometric word theory. In recent years, a surge of research has delved into the realm of fine-grained and hierarchical shape segmentation. Yi et al. [41] leveraged noisy part decomposition derived from CAD model designs to learn consistent shape hierarchies. Furthermore, a recursive binary decomposition network [42] was introduced to address shape hierarchical segmentation challenges in a recursive manner.

III. OUR APPROACH

This section offers a comprehensive introduction to our approach, as illustrated in Fig. 2. The complete framework consists of three core steps:

- **Construction of the 3D Shape Knowledge Graph:** The initial step involves generating multiple images from various viewpoints of 3D shapes. Subsequently, we employ an image segmentation technique [43] to partition each rendered image into distinct shape parts. These segmented parts are then categorized into a collection of geometric words, allowing for the projection of each shape component into a corresponding geometric word. Additionally, we establish entities and edges to facilitate the construction of the 3D shape knowledge graph.
- **Graph Embedding:** Our approach introduces a graph embedding strategy tailored to the structure of our 3D shape knowledge graph. Notably, we define the category edge within the knowledge graph. This edge's manipulation enables our approach to effectively address both supervised and unsupervised problems.
- **Similarity Measure:** Drawing on the entity embeddings, we put forth an efficient similarity measurement method. This method encompasses various similarity measurement strategies, as depicted in Fig. 2. Further elaboration on these steps can be found in Subsection III-D.

The ensuing sections will provide a detailed breakdown of each of these steps, elucidating our approach's intricacies and contributions.

A. Data Preprocessing

Data processing plays a pivotal role in our approach, focusing on the crucial task of identifying visual geometric words to construct the 3D shape knowledge graph. This process encompasses three distinct steps: 1) **Extraction of Rendered Views:** Starting with a 3D model, we extract multiple rendered views. Each 3D model generates a corresponding set of images. 2) **Image Segmentation:** We apply an image segmentation technique to segment the rendered images. Each object is dissected into a collection of parts, with each part associated directly with its corresponding rendered image. 3) **Part Classification for Geometric Words:** Subsequently, we classify these parts to extract essential information. The objective here is to discern the geometric words, with each class representing a distinct geometric word. The central point of each part serves as the representative of its associated geometric word.

In the course of this process, our focus rests on 2D object segmentation techniques [44]. Classic 3D shape decomposition methods or unsupervised techniques such as those in [34, 45, 46] do not apply in this context. The absence of an

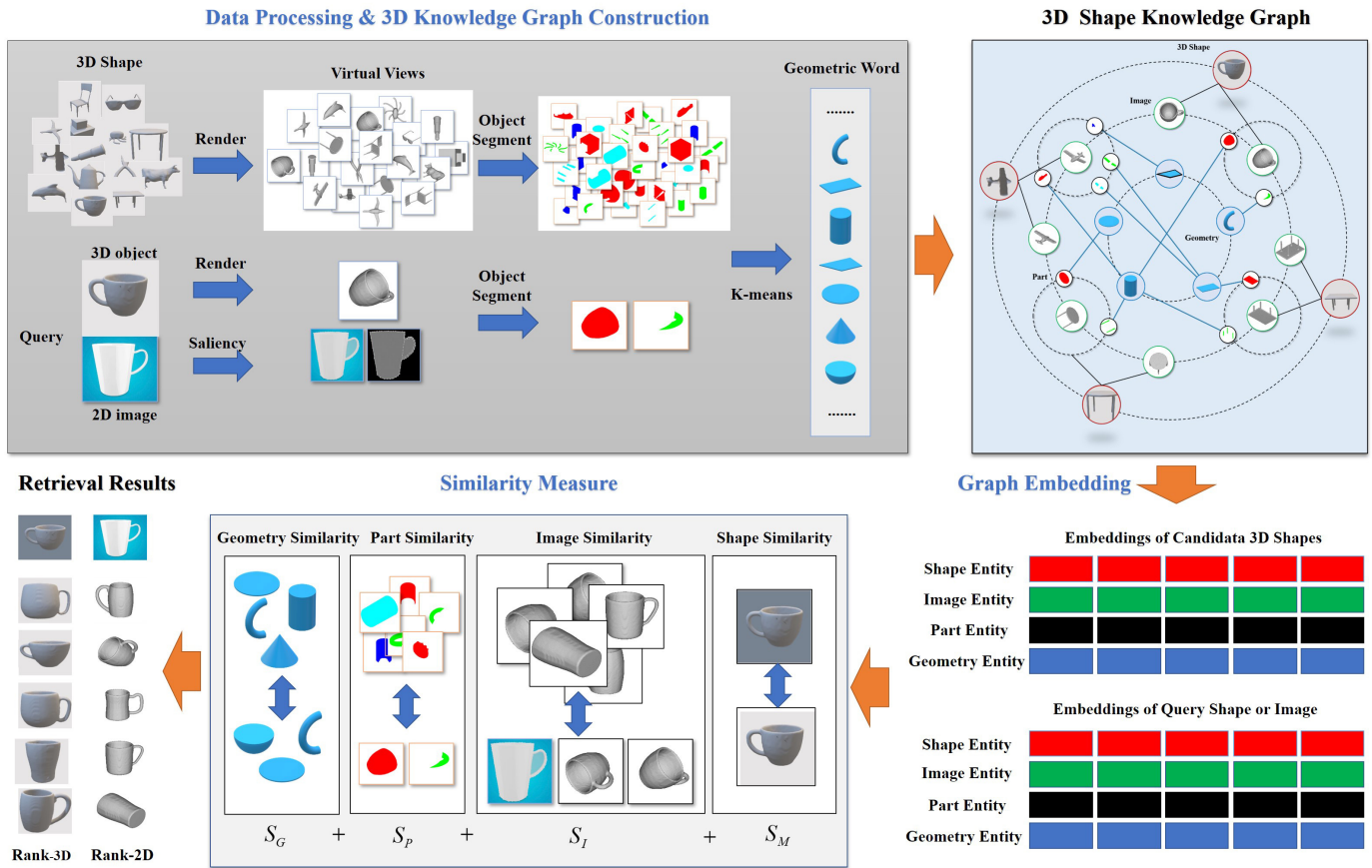


Fig. 2. The framework of our approach, which includes three parts: knowledge graph construction (entity and edge extraction), graph embedding and similarity measure. K-means is used to generate geometric descriptions. The embedding strategy embeds the graph entities into vector space for retrieval.

effective method for object segmentation led us to develop a new 3D shape segmentation dataset. To train the segmentation model, we employed the well-established FCN model [43]. The segmentation dataset, as depicted in Fig. 3, along with its detailed specifications available in the supplemental files, has been made publicly accessible on GitHub². We employed the classic FCN model [43] for training, utilizing 4,940 samples for training, 1,900 for validation, and 760 for testing. Notably, Fig. 4 showcases select segmentation results. During training, unlike traditional segmentation models, our approach doesn't require object-specific label information, relying solely on the ground truth of segmentation. This implies that the segmentation model trained using our dataset serves as a general segmentation tool applicable to diverse shapes. This process ultimately yields a collection of shape parts associated with each rendered or real image, as illustrated in Fig. 4. Several well-regarded segmentation techniques were also employed for comparative analysis. The outcomes of these experiments are presented in Table I. The retrained model exhibits superior performance. Through these processes, we attain sets of rendered images, shape parts, and geometric words, each with explicit correlations. This valuable information forms the foundation for constructing the 3D shape knowledge graph. Importantly, it's worth acknowledging that segmentation methods serve as

preprocessing steps. Their performance significantly influences the eventual outcomes of retrieval and classification. While other segmentation methods could be employed, we have selected the most effective approach for our subsequent work.

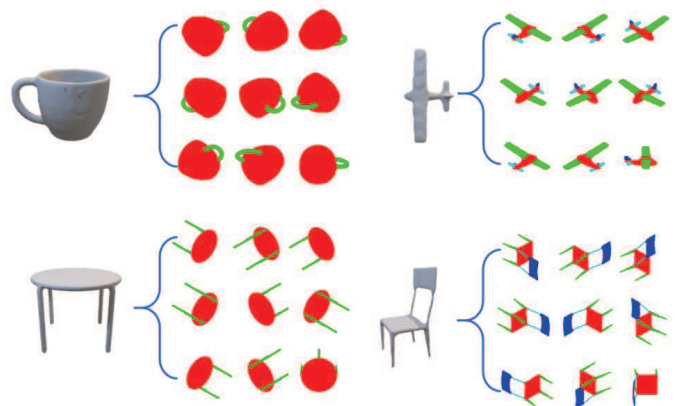


Fig. 3. Some training examples in the object segmentation dataset

B. 3D Shape Knowledge Graph Construction

This section elucidates the meticulous process of constructing the 3D shape knowledge graph, which necessitates the definition of entities and their associated edge information. The

²Removed for anonymized peer review

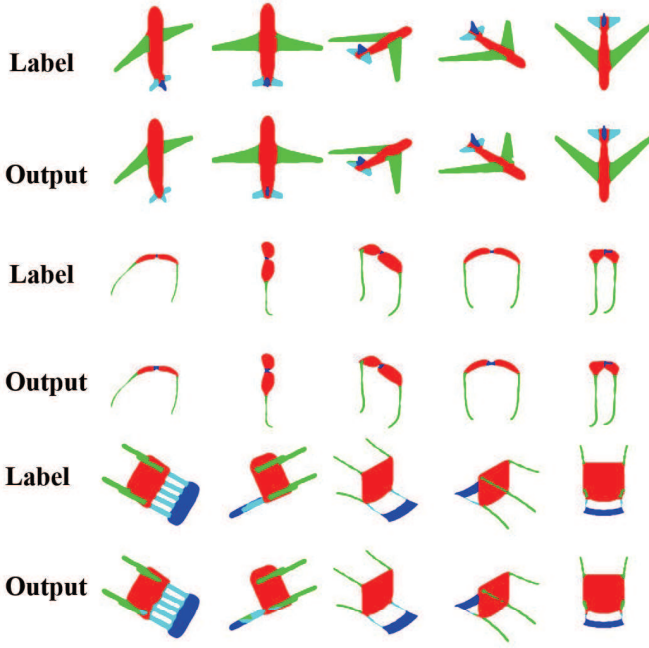


Fig. 4. Some segmentation results based on the FCN

TABLE I
PERFORMANCE COMPARISONS OF THE FCN WITH OTHER CLASSICAL
METHODS ON OUR DATASET

<i>Model</i>	<i>Backbone</i>	<i>MIoU</i>
U-Net[47]	-	80.68
SegNet[48]	VGG16	82.84
PSPNet[49]	ResNet-103	86.49
DeepLab v3[50]	ResNet-101	90.42
FCN	VGG16	96.09

sufficiency of edges or relations within the graph significantly impacts the representation of the 3D shape, as limited information hinders the effective learning of entities. Hence, the architectural structure of the knowledge graph is of paramount importance, and this process is detailed comprehensively below.

Entity Definitions in the 3D Shape Knowledge Graph:

1. **Model Entity:** This entity embodies the query 3D shape. We employ PointNet++ [13] to extract feature vectors for each shape and subsequently integrate them into G . To maintain uniform dimensionality of shape descriptors, PCA [51] is applied for feature vector dimension reduction.

2. **Image Entity:** This entity represents rendered images derived from the 3D shape. Furthermore, it can represent real images if the knowledge graph is used for cross-modal 3D shape retrieval. We utilize two methodologies for extracting rendered images, as delineated in Fig. 5. For Case C1, we employ NPC [52] to orient the 3D shape upright along a fixed axis (e.g., z-axis). Cameras are then positioned at a fixed angle θ around this axis, set at 30 degrees from the ground plane, and facing the shape’s center. Different θ values generate varying views, producing $\{20; 16; 12; 10; 8; 6; 4; 2; 1\}$ views for each object. In Case C2, a diverse perspective is adopted, where shapes are not continuously kept upright. Instead, multiple

views are sampled from the 3D space. Specifically, we deploy 20 virtual cameras at the vertices of a dodecahedron shape situated around the object’s center.

3. **Part Entity:** Based on rendered or real images, each image is segmented into parts using a model trained on our dataset [43]. These segmented parts serve as part entities, representing the attributes of each shape in the knowledge graph. Real images require additional preprocessing due to complex backgrounds, where salient object detection [53] is applied to separate the object from the background.

4. **Geometric Word Entity:** These entities serve as pivotal elements in the 3D shape knowledge graph, bridging the gap between disparate domains or modalities. Geometric word entities are generated from part entities originating from different images, including rendered images and real images representing the same object. Similar part entities are categorized as geometric words. We employ a pretrained CNN [54] to generate descriptors, followed by K-means clustering to determine geometric word labels, with their centers serving as descriptors.

Edge Definitions in the Knowledge Graph :

1. **Lash Edge:** This edge establishes connections between the 3D shape and its rendered images, rendered images and segmented parts, and real images and segmented parts. Such connections embody the geometric and visual attributes of the 3D shape within G .

2. **Geometric Edge:** This edge links part entities to their respective geometric word entities, reflecting the geometric structure of the 3D shape or real image.

3. **Category Edge:** Capturing inter-category relations, this edge represents a priori knowledge. Its presence allows our approach to function in a supervised manner. Removal of this edge renders our approach unsupervised.

In summary, the knowledge graph G holistically captures the geometric structure and categorical information of 3D shapes. Each edge encapsulates distinct knowledge, e.g., "table, rectangle, lash" signifying the presence of a rectangle within a table. Notably, entities (3D shapes, 2D images, geometric words) lack explicit text labels. As depicted in Fig. 1, the segmentation process indirectly illustrates the composition of the knowledge graph.

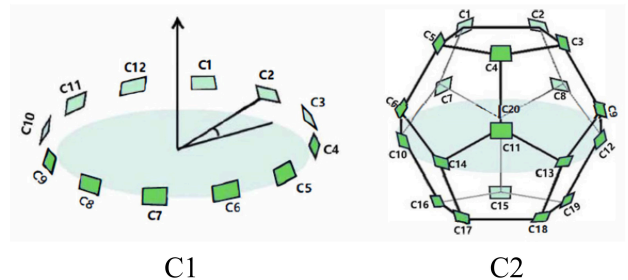


Fig. 5. Illustration of classic viewpoint setups. Both of C1 and C2 center the 3D object and surround the object with cameras for comprehensive views.

C. Graph Embedding

Up to this point, we have successfully constructed the 3D shape knowledge graph. To effectively address the challenges of cross-domain 3D shape retrieval, we must devise a strategy to generate embeddings for each node based on the structure of this knowledge graph. This section provides an in-depth explanation of our innovative embedding approach.

1) *Problem Definition:* The 3D shape knowledge graph captures the structural aspects of 3D shapes and directly reveals the correlation between visual information and 3D shapes. However, it does not fully address the weak correlation that exists in (Euclidean) space between a real image and a 3D shape. Consequently, employing a graph embedding technique to create dense embedding features for sparse data becomes a compelling avenue.

In this study, we introduce a novel graph convolutional network to generate node embeddings, thereby leveraging the structure of the 3D shape knowledge graph, particularly the geometric word, to enhance feature vector consistency between similar 3D shapes and to establish connections between images and 3D shapes.

We define the knowledge graph as an undirected weighted graph $G = (V, E)$, where V denotes the nodes and E represents the edges. Specifically, we divide the node set V into five distinct parts: $V = V^M, V_v^I, V_r^I, V^P, V^G$, where V^M signifies the model entity set, V_v^I corresponds to the rendered image entity set, V_r^I pertains to the real-image entity set, V^P encompasses the part shape entity set, and V^G represents the geometric word entity set. Formally, our problem can be articulated as follows: given an undirected weighted graph $G = (V, E)$ and the node feature matrix $X \in \mathbb{R}^{N \times K}$, wherein each node is represented by an N -dimensional feature vector and K signifies the number of entities in G , our objective is to learn embeddings for all nodes within the graph. The final node embedding in graph G is denoted as $X \in \mathbb{R}^{E \times K}$, where each node boasts an E -dimensional embedding. Our ultimate optimization objective can be expressed as follows:

$$\min \sum_{v_i, v_j \in V} -\log p(1|v_i, v_j) + \log p(0|v_i, v_j), \text{ s.t } v_i \neq v_j, \quad (1)$$

Here, $p(1|v_i, v_j)$ signifies the presence of a direct edge between nodes v_i and v_j in graph G , while $p(0|v_i, v_j)$ indicates the absence of an edge between them. The objective aims to minimize the direct distance between similar nodes. In scenarios where specific category information about the 3D shape or 2D image is available, additional category edges are introduced between relevant entities. These edges serve to reduce the distance between embeddings of two entities. Furthermore, if a 3D shape and a 2D image share the same geometric word entity, they are connected via a pathway consisting of multiple edges. This information, integrated into the graph embedding process, mitigates disparities between entities, ultimately influencing the final entity embeddings.

In summary, our approach involves generating embeddings for nodes within the 3D shape knowledge graph. This is achieved by utilizing a novel graph convolutional network that leverages the graph's structural characteristics, particularly

the geometric word entity, to enhance the consistency of feature vectors for similar 3D shapes and establish meaningful connections between images and 3D shapes. The objective function minimizes the direct distance between related nodes and incorporates category edges and geometric word entities to facilitate effective cross-domain retrieval.

2) *Graph Neural Network:* As highlighted in the literature, graph neural networks (GNNs) have emerged as a potent and contemporary approach for acquiring representations within graph structures [55]. Consequently, we place a pronounced emphasis on the application of Graph Convolutional Networks (GCNs) for embedding the 3D shape knowledge graph. Our primary objective revolves around addressing the challenges associated with cross-domain 3D shape retrieval. In this context, the utilization of GCNs is specifically directed towards enhancing the representation learning process for both shape entities and image entities. It is pertinent to note that these distinct entities inherently possess diverse representations and interact with different sets of neighbors.

Within the context of our knowledge graph, an essential principle is that images and 3D shapes representing the same object should share corresponding geometric entities. This underlines the importance of employing geometric entities to facilitate the generation of embeddings for both image and shape entities. By doing so, we aim to ensure that entities corresponding to identical objects exhibit embeddings that are coherent and comparable. In essence, our approach underscores the pivotal role of Graph Convolutional Networks (GCNs) in addressing the intricacies of cross-domain 3D shape retrieval. This entails leveraging shared geometric entities to underpin the embedding process for image and shape entities, thus establishing a robust and unified foundation for effective representation learning within the 3D shape knowledge graph.

The classic GCN structure[55] is used to learn the embeddings of the nodes, which is defined as follows:

$$y^{(l+1)} = \text{Relu}(\tilde{D}^{-\frac{1}{2}} \tilde{A} \tilde{D}^{-\frac{1}{2}} y^{(l)} W^{(l)}), \quad (2)$$

where $y^{(l+1)} \in \mathbb{R}^{N \times F}$ is the final entity feature matrix in graph G . The subscript l is the index of the domain-shared layer. The term N represents the entity number on the knowledge graph. Let A be the original adjacency matrix. The graph adjacency matrix is calculated as $\tilde{A} = A + I_N \in \mathbb{R}^{N \times N}$. The learned weight of the l -th GCN layer is $W^{(l)}$. Finally, the embeddings $y^{(l+1)}$ is generated by combining all the entity embeddings. The adjacency matrix $\tilde{D} \in \mathbb{R}^{N \times N}$ is calculated as follows.

$$\tilde{D}(i, j) = \sum_j \tilde{A}(i, j). \quad (3)$$

To learn the embeddings of an entity, we train the neural network by modeling the graph structure. We use the embeddings to generate the linkage between two entities, i.e., the probability that there exists an edge between v_j and v_i in Eq.1. Therefore, we formulate embedding learning as a binary classification problem by using the embeddings of two entities.

The probability that there exists an edge between node v_i and node v_j in graph G is defined in Eq.4 and the probability

Algorithm 1 Graph Convolutional Network

Input: Graph $G = (V, E)$, the node feature matrix $X \in \mathbb{R}^{N \times M}$, and the initialized parameter W .

Output: The learned parameter W and the embeddings Y .

- 1: Initialize parameters W ,
 - 2: **for** $(v_i, v_j) \in \mathbf{S}$ **do**
 - 3: Sample a set of samples S .
 - 4: Compute Gradients: $\frac{\partial L(W)}{\partial W}$.
 - 5: Update $W' = W - b \frac{\partial L(W)}{\partial W}$.
 - 6: **return** The final embeddings: Y .
-

that there exists no edge between node v_i and node v_j in graph G is defined in Eq.5.

$$p(1|v_i, v_j) = \sigma(y_i^T \dot{y}_j), \quad (4)$$

$$p(0|v_i, v_j) = \sigma(-y_i^T \dot{y}_j), \quad (5)$$

where y_i is the embedding vector of v_i , and \dot{y}_j is the embedding vector of v_j . $\sigma(\cdot)$ is the sigmoid function.

Accordingly, the optimization objective function Eq.1 is expressed as:

$$\begin{aligned} & \min_{v_i, v_j \in V} -\log p(1|v_i, v_j) + \log p(0|v_i, v_j) \\ = & \min - \sum_{v_j \in S_p} \log p(1|v_i, v_j) + \sum_{v_k \in S_n} \log p(0|v_i, v_k) \quad (6) \\ = & \min - \sum_{v_j \in S_p} \log \sigma(y_i^T \cdot y_j) + \sum_{v_k \in S_n} \log \sigma(y_i^T \cdot y_k), \end{aligned}$$

where S_p is the set of entities in graph G that has a clear pathway to node v_i , and S_n is the set of nodes that does not have a pathway to node v_i . Thus, the final objective function is defined as:

$$L = \min - \sum_{v_j \in S_p} \log \sigma(y_i^T \cdot y_j) + \sum_{v_k \in S_n} \log \sigma(y_i^T \cdot y_k). \quad (7)$$

3) *Optimization:* In our model, we need to find the optimized parameter W . The classic back-propagation algorithm is utilized to optimize this parameter. Thus, the optimization objective is defined as follows:

$$\begin{aligned} W^* &= \arg \min_W L(W) \\ &= \arg \min_W - \sum_{v_j \in S_p} \log \sigma(y_i^T \dot{y}_j) + \sum_{v_k \in S_n} \log \sigma(y_i^T \dot{y}_k). \end{aligned} \quad (8)$$

The goal of this objective function is to find the solution that is optimal for each entity representation. W is trained by the optimizer according to the gradient: $W' = W - b \frac{\partial L(W)}{\partial W}$. Here, we summarize the learning procedure of our approach in Algorithm 1. We first input the graph G , the input feature X and the initialization parameter W . Then, we sample the training samples S . v_i and v_j are sampled from S . The existing pathways are utilized for the training of the network, compute the gradients and update the parameters of the specific graph convolutional layers. Finally, we return a set of embeddings for each entity.

D. Similarity Measure

Based on the above process, a 3D shape knowledge graph and corresponding entity embeddings are generated. The next issue is how to manage the similarity measure between the candidate shapes and the query shape/image according to these embeddings. In this section, we will detail our solution.

Given a query shape Q , the query image I and a large 3D shape dataset \mathbb{M} , the purpose of 3D shape retrieval is to construct a similarity measure function to calculate the similarity between query shape Q , query picture I and candidate shape $M \in \mathbb{M}$. In this work, we first build the 3D shape knowledge graph on the dataset \mathbb{M} , query shape Q and query image I . Then, the GCN model is utilized to generate the related embeddings for each entity. Finally, we measure the similarity between Q/I and M according to these embeddings.

For each query shape Q , the directly related entities include image entities, part entities and geometric entities, as shown in Fig.1. These entities can be represented by a set of embeddings, as shown in Fig.6. Here, we utilize I_Q to represent the image entity set, P_Q to represent the part entity set and G_Q to represent the geometric word entity set. Each entity will be represented by an embedding. Here, f is utilized to represent the embedding of each entity. Thus, for the query shape Q , the image entity set can be represented as $I_Q = \{f_1^{I_Q}, f_2^{I_Q}, \dots, f_n^{I_Q}\}$, the part entity set can be represented as $P_Q = \{f_1^{P_Q}, f_2^{P_Q}, \dots, f_m^{P_Q}\}$, and the geometric word entity set is represented as $G_Q = \{f_1^{G_Q}, f_2^{G_Q}, \dots, f_l^{G_Q}\}$. Each candidate shape M can also be represented by the related image entity, part entity and geometric entity. Here, we utilize I_M , P_M and G_M to represent the three kinds of entity sets. Meanwhile, $I_M = \{f_1^{I_M}, f_2^{I_M}, \dots, f_n^{I_M}\}$, $P_M = \{f_1^{P_M}, f_2^{P_M}, \dots, f_m^{P_M}\}$ and $G_M = \{f_1^{G_M}, f_2^{G_M}, \dots, f_n^{G_M}\}$ are utilized to represent the embeddings of the candidate shapes. The objective is to calculate how similar Q and M are. We first define the similarity between two different entities by Eq.9.

$$S_e(e_i, e_j) = \frac{1}{2}(1 + \cos(f_{e_i}, f_{e_j})), \quad (9)$$

where f_{e_i} and f_{e_j} are the embedding features of entities e_i and e_j . Here, the classic cosine distance is utilized to compare different entities. The cosine distance has the range $[-1, +1]$. Eq.9 is utilized for normalization.

Then, according to different entities, the similarity between query shape Q and candidate shape M is defined as:

$$\begin{aligned} S(Q, M) &= \alpha S_M(f_Q, f_M) + \beta S_I(I_Q, I_M) \\ &\quad + \gamma S_P(P_Q, P_M) + \lambda S_G(G_Q, G_M), \quad (10) \\ & \text{s.t. } \alpha + \beta + \gamma + \lambda = 1, \end{aligned}$$

where f_Q and f_M are the embeddings of the query shape entity and the candidate shape entity, respectively. $S_M(f_Q, f_M) = S_e(f_Q, f_M)$. Meanwhile,

$$S_I(I_Q, I_M) = \max_{i=1, j=1}^{n, m} S(f_i^{I_Q}, f_j^{I_M}), \quad (11)$$

where n and m are the number of image entities in I_Q and I_M , respectively.

$$S_G(G_Q, G_M) = \text{sigmoid}(\log(M_w \cap Q_w)). \quad (12)$$

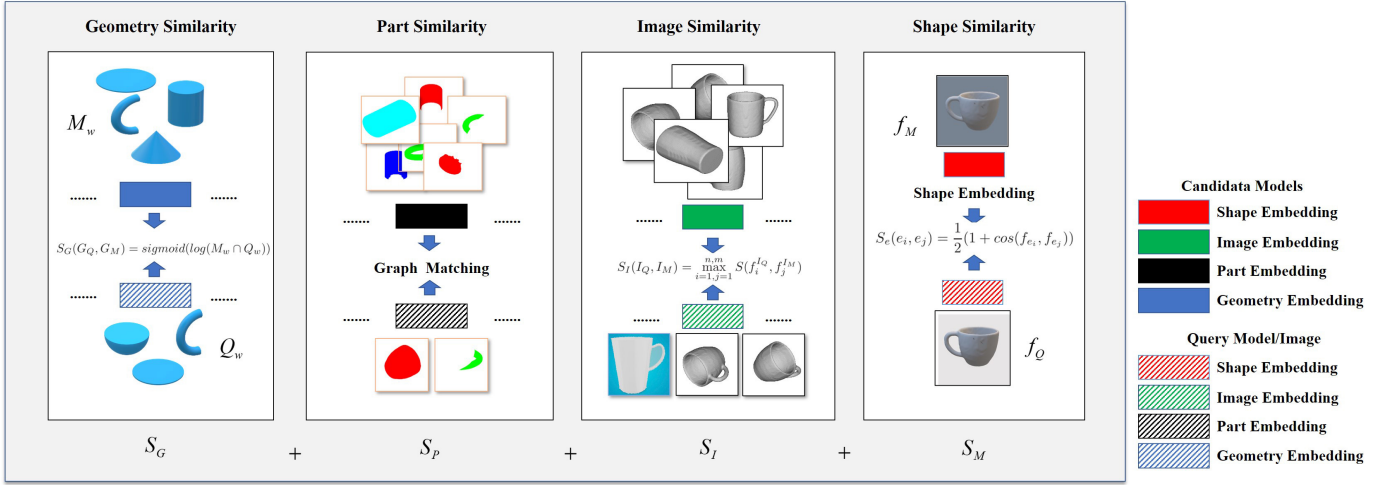


Fig. 6. Illustration of the similarity measure. S_M denotes the 3D-shape-level similarity measure, S_I denotes the view-level similarity measure, S_P denotes the part-level similarity measure and S_G denotes the geometry-word-level similarity measure.

For $S_P(G_Q, G_M)$, we adopt the bipartite graph matching method [56] for the similitude measurement between different part entity sets. However, the results of graph matching are a set of matching pairs. The matching score is the summary of matching pairs. Here, we normalize the results by combining averages. α , β , γ and λ are the weights of these four similarity measures, which are used to control the contributions of different entities in the measurement.

In other words, for each query image I , the directly related entities include part entities and geometric word entities. These entities can be represented by a set of embeddings. Here, P_I and G_I are utilized to represent the part entity set, and the geometric word entity set, respectively. We also utilize $P_I = \{f_1^{I_Q}, f_2^{I_Q}, \dots, f_n^{I_Q}\}$ and $G_I = \{f_1^{I_Q}, f_2^{I_Q}, \dots, f_n^{I_Q}\}$ to represent the embeddings of these two kinds of entities. The final similitude between the input image and its relevant shape can be calculated as:

$$S(I, M) = \beta^* S_I(f_I, I_Q) + \gamma^* S_P(P_I, P_M) + \lambda^* S_G(G_I, G_M), \quad (13)$$

$$s.t. \quad \beta^* + \gamma^* + \lambda^* = 1,$$

where f_I is the input query (image) embedding. I_Q is the candidate 3D shape's view embedding set.

$$S_I(I, I_M) = \max_{j=1}^m S(f_I, f_j), \quad (14)$$

where m is the number of views extracted from the candidate 3D shape M . $S_G(G_Q, G_M)$ is computed by Eq.12. For $S_P(P_Q, P_M)$, we applied a computational approach similar to shape retrieval. β^* , γ^* , and λ^* are the weights of these three similarity measures in Eq. 13, which are also used to balance the contributions of different entities in the final similarity measure.

So far, we are able to handle the 3D shape retrieval and cross-domain 3D shape retrieval without massive training and parameter debugging issues. We only focus on how to enlarge the size of the geometric words in the proposed knowledge graph.

IV. EXPERIMENT AND DISCUSSION

We have conducted a comprehensive set of experiments to showcase the efficacy of our proposed approach. Section IV-C presents the experimental outcomes pertaining to the conventional 3D shape retrieval task, utilizing the widely-recognized ModelNet40 dataset. In Section IV-D, our focus shifts towards evaluating the performance in the context of cross-domain retrieval. In this scenario, we utilize 3D shapes extracted from the ModelNet40 test set as queries, seeking similar 3D shapes from the Shapenet-Core-55 dataset [12]. Furthermore, we delve into the realm of cross-modal retrieval in Section IV-E, where we present our experimental investigations. In contrast to the aforementioned experiments, this scenario involves utilizing an input image as the retrieval query, with the corresponding 3D shapes serving as the retrieval targets. The subsequent subsections will provide a comprehensive breakdown of these experiments, offering intricate insights into each facet of our evaluation process.

A. Dataset

To evaluate the efficiency of our proposed method, we made considerable use of ModelNet40[12] dataset, which contains 12,311 CAD models divided into 40 categories. ModelNet40's training and testing data are made up of 9,843 and 2,468 3D models, respectively. This dataset is utilized to find the best parameters of our model. To demonstrate our approach on the cross-domain information retrieval task, we use the ShapeNet-Core-55 dataset. This dataset has been used for the Shape Retrieval Contest (SHREC) 2018 competition track to evaluate the performance of 3D shape retrieval methods. Our method for cross-modal 3D shape retrieval is also shown using the MI3DOR dataset from SHREC 2018. This dataset, which includes 21,000 2D monocular photos of 21 categories and 7,690 3D shapes, is a public benchmark for 3D shape retrieval using monocular images that was provided by [57]. The benchmark is split into two sets: a training set that comprises 3,842 3D shapes and 10,500 2D images, and a

testing set that uses the remaining data. We have conducted extensive experiments to evaluate the performance of our method. However, due to the length constraints, we only select some key experiments to describe in the manuscript. More experiments are shown in supplemental files.

B. Evaluation Metrics

In the context of 3D shape retrieval, the credibility of our experimental outcomes hinges upon the thoroughness of our evaluation methodology. To this end, we employ a range of well-established metrics [58], including but not limited to nearest neighbor (NN), first tier (FT), second tier (ST), F-measure (F), and discounted cumulative benefit (DCG). By applying these metrics, we rigorously assess the performance of our approach against state-of-the-art methods, facilitating a comprehensive and insightful comparative analysis.

C. 3D shape representation on ModelNet40

In order to validate the efficacy of our proposed method, we conducted comprehensive 3D shape retrieval experiments utilizing the Princeton ModelNet40 dataset [12]. Our comparisons encompass a diverse array of methodologies, spanning different representations of 3D data. These include volumetric-based techniques [12], handcrafted features tailored for multi-view data [59] [17], deep learning approaches designed for multi-view data [3] [60], deep learning methods tailored for panorama views [19], as well as point cloud-based methodologies [6] [13] [61]. Through these extensive comparisons, we aim to establish a robust assessment of our approach’s performance.

TABLE II
EXPERIMENTAL RESULTS OF 3D SHAPE CLASSIFICATION AND RETRIEVAL ON MODELNET40.

Method	Classification (ACC)	Retrieval (mAP)
SPH[59]	68.2%	33.3%
LFD[62]	75.5%	40.9%
3D ShapeNets[12]	77.3%	49.2%
VoxNet[63]	83.0%	-
VRN[64]	91.3%	-
MVCNN (AlexNet)[3],	89.5%	80.2%
MVCNN (GoogLeNet),	92.2%	83.0%
LMVCNN-VggNet-11[65],	93.5%	-
VS-MVCNN[66]	90.9%	-
PointNet++[13]	90.7%	-
DGCNN[61]	92.2%	-
PVNet[8]	93.2%	89.5%
N-gram Network[67]	90.2%	89.3%
PCT[68]	93.2%	-
Ours (AlexNet), 12×	93.7%	91.8%
MLVACN[69]	-	93.5%
Ours (ResNet), 12×	96.9%	92.7%

In our study, we utilized the test data as the query models, while the training data was employed to construct the 3D shape knowledge network. The comparative evaluation against state-of-the-art methods is summarized in Table II. In the context of the 3D classification task, our approach demonstrates superior performance. Notably, our approach outperforms Point Cloud Transformer (PCT)[68] by a margin of 3.7%. Additionally, in

addressing the retrieval problem, our approach also achieves favorable results. Remarkably, in contrast to traditional methods, our approach circumvents the need for an intricate training process, the benefits of which will be exhibited in the next subsection.

D. 3D shape retrieval based on cross-domain datasets

The 3D shape knowledge graph proves to be a highly effective solution for addressing the cross-domain 3D shape retrieval challenge. A characteristic form of this cross-domain predicament involves learning from data that adheres to dissimilar distributions. To elucidate this concept, we employ 3D shapes from the ModelNet40 testing set as query models, seeking related 3D shapes from the ShapeNet-Core-55 dataset. The ensuing experimental results substantiate the efficacy and resilience of the 3D shape knowledge graph, as exemplified in Table III. For the purpose of comparison, we have implemented several standard cross-domain learning methodologies[10, 70–73]. These approaches involve mapping cross-domain embeddings onto an intermediary domain and subsequently gauging their similarity using the Euclidean distance metric.

Significantly, our approach dispenses with the need for training, setting it apart from these cross-domain learning methods. In this context, we directly evaluated our performance without any training or fine-tuning interventions. As evidenced by the data presented in Table III, the disparity in performance between state-of-the-art (SOTA) methods and our approach is negligible. Nonetheless, even though our method is applied to the cross-domain dataset without training, it is still successful in addressing the cross-domain retrieval task and is comparable to or outperforms other state-of-the-art methods.

TABLE III
EXPERIMENTAL RESULTS ON THE CROSS-DOMAIN DATASET (TRAINED ON THIS TASK). QUERIES ARE FROM MODELNET40 AND CANDIDATES ARE RETRIEVED FROM SHAPENET.

Method	NN	FT	ST	F	DCG	ANMRR
RevGard[70]	0.89	0.79	0.90	0.33	0.83	0.15
JAN[71]	0.90	0.81	0.91	0.33	0.84	0.14
TJM[10]	0.90	0.81	0.91	0.34	0.84	0.14
JDA[73]	0.91	0.82	0.91	0.34	0.85	0.14
JGSA[72]	0.92	0.82	0.92	0.34	0.85	0.13
KGMR[33]	0.91	0.83	0.92	0.34	0.87	0.13
IPSC[74]	0.93	0.83	0.93	0.36	0.87	0.12
SI3DMR[75]	0.94	0.84	0.93	0.35	0.88	0.10
Ours	0.93	0.84	0.94	0.36	0.87	0.12

E. 3D shape retrieval on cross-modal conditions

The cross-domain situations are currently narrowed as cross-modal conditions in 3D shape retrieval tasks. To verify the performance of the proposed method on the cross-modality information retrieval, we also conduct experiments on a dataset more suitable for this task, SHREC 2019 Monocular Image-Based 3D Object Retrieval (MI3DOR) [57]. The comparison methods on the MI3DOR dataset involve both supervised and unsupervised methods. They are distinguished by whether labels are available for the target domain data. We compare

our approach with both kinds of these methods. The related experimental results are listed in Table.IV for supervised methods and Table.V for unsupervised methods. According to the results, our method achieves promising results. The results demonstrate the performance of various methods on the MI3DOR dataset, focusing on cross-modal retrieval, which is similar to image-based 3D shape retrieval. In the supervised methods, our method consistently outperforms other techniques across most metrics. It achieves the highest retrieval rates, indicating its effectiveness in retrieving relevant 3D shapes.

The unsupervised methods also highlight the competitiveness of the proposed method. While it may not achieve the highest values in all metrics, it still maintains strong performance across the board. Notably, in the unsupervised setting, our method performs comparably or better than most other methods, and it achieves the best F_measure, indicating a better ranking of retrieved shapes.

Overall, the experimental results suggest that the proposed method, which leverages a 3D shape knowledge graph with integrated geometry information, yields favorable cross-modal retrieval performance in both supervised and unsupervised scenarios on the MI3DOR dataset. This integration of geometry-based knowledge into the knowledge graph seems to contribute positively to the retrieval of relevant 3D shapes, making the proposed method a promising approach for 3D shape retrieval tasks.

TABLE IV
EXPERIMENTAL RESULTS OF SUPERVISED METHODS ON MI3DOR DATASET. ALL METHODS FOR COMPARISON ARE FROM SHREC 2019 MONOCULAR IMAGE-BASED 3D OBJECT RETRIEVAL (MI3DOR) [57]

Method	NN	FT	ST	F	DCG	ANMRR
RNF-MVCVR	0.97	0.92	0.93	0.2	0.93	0.06
SORMI	0.94	0.92	0.96	0.18	0.92	0.07
RNFETL	0.97	0.91	0.97	0.18	0.92	0.07
CLA	0.95	0.88	0.89	0.2	0.9	0.1
MLIS	0.94	0.91	0.96	0.18	0.91	0.08
ADDA-MVCNN	0.87	0.86	0.87	0.17	0.87	0.13
SRN	0.89	0.86	0.87	0.18	0.88	0.12
ALIGN	0.64	0.69	0.8	0.13	0.69	0.3
Ours	0.98	0.93	0.98	0.21	0.94	0.06

TABLE V
EXPERIMENTAL RESULTS OF UNSUPERVISED METHODS ON MI3DOR DATASET.

Method	NN	FT	ST	F	DCG	ANMRR
MEDA[76]	0.43	0.34	0.50	0.05	0.36	0.65
JMMD-AlexNet[57]	0.44	0.34	0.49	0.08	0.364	0.64
JAN[71]	0.45	0.34	0.50	0.09	0.36	0.65
MVML[57]	0.61	0.44	0.59	0.11	0.47	0.54
JGSA[72]	0.61	0.44	0.60	0.12	0.47	0.54
IPSC[74]	0.73	0.65	0.81	0.15	0.67	0.34
S3DMR[75]	0.78	0.58	0.73	0.15	0.62	0.40
Ours	0.64	0.47	0.62	0.17	0.53	0.49

F. Discussion on Similarity Measurement

In this section, we present a comprehensive similarity calculation method that encompasses various entities, as illustrated

in Fig.6. To evaluate the efficacy of our proposed approach, we conducted a thorough comparative analysis involving different similarity measures, using the ModelNet40 dataset as our experimental platform. The results of these experiments are summarized in Table.VI.

From the experimental outcomes, it is evident that the supervised method outperforms the unsupervised alternatives. This superiority can be attributed to the inclusion of the category edge within the 3D shape knowledge graph. The additional information introduced by the category edge contributes to the enhancement of the embedding quality produced by the GCN method. In other words, our amalgamated similarity measure achieves the most favorable retrieval results. However, among the single similarity measures, S_M stands out by yielding the most promising outcomes. Nevertheless, in the context of unsupervised methods, S_G manages to achieve a slight improvement over other single similarity measures. This discrepancy can be attributed to the reliance of the graph embedding method on category information during the supervised learning stage. The category edge establishes a clear path between relevant entities, thereby fortifying their relationships. Consequently, S_P , S_I , and S_M contribute more information to the similarity measure. In unsupervised learning scenarios, the absence of the category edge in the 3D shape knowledge graph places greater emphasis on the geometric entity as the sole bridge between disparate shapes and different modalities. This entity assumes a pivotal role in the graph embedding process, causing the information conveyed by S_P , S_I , and S_M to converge toward S_G , as revealed through the graph embeddings operation. These findings are consistently supported by the final experimental results.

Building upon these insights, we introduce weighted coefficients for each similarity measure in the final step of similarity fusion. Specifically, under the supervised setting, the weights assigned to the four similarity measures (S_G , S_P , S_I , and S_M) are 0.1, 0.3, 0.2, and 0.4, respectively, when the query pertains to a 3D shape. When the query involves a 2D image, the weights for the three similarity measures (S_G , S_P , and S_I) are set at 0.2, 0.4, and 0.4, respectively. In the unsupervised scenario, the weights for the four similarity measures (S_G , S_P , S_I , and S_M) are adjusted to 0.3, 0.2, 0.2, and 0.3, respectively, for 3D shape queries. Similarly, for 2D image queries, the weights for the three similarity measures (S_G , S_P , and S_I) are fine-tuned to 0.3, 0.2, and 0.4, respectively.

G. Discussion on the Geometric Word Entities

In this section, we introduce a crucial element of our proposed framework - the geometric word entity, which serves as the cornerstone of our 3D shape knowledge graph and functions akin to a dictionary for object representation. As such, the dimensionality of this dictionary plays a pivotal role in our entire framework and wields a direct impact on the ultimate performance. To shed light on this dimensionality's influence, we conduct comparative experiments with varying numbers of geometric word entities and present the results in Table VII.

To gauge the efficacy of our approach in the context of the retrieval task, we leverage the ModelNet40 dataset. Observing

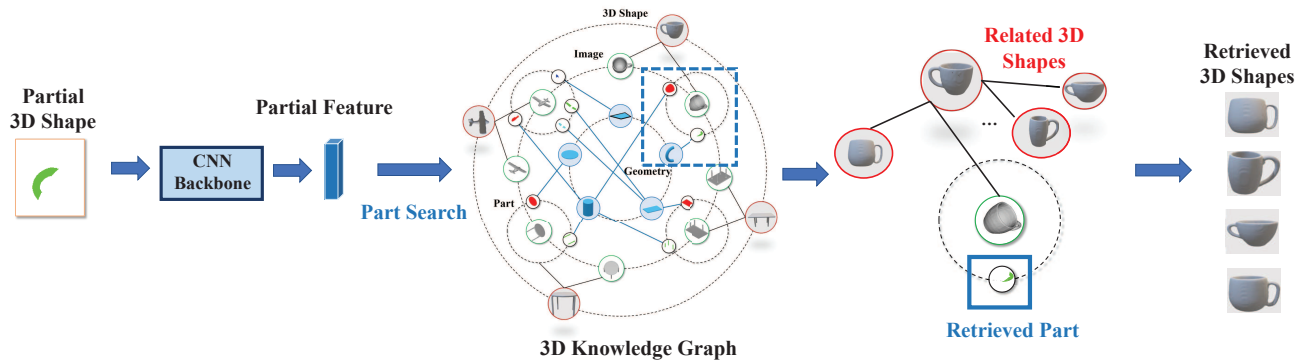


Fig. 7. Partial 3D model retrieval framework.

TABLE VI
COMPARISON OF DIFFERENT SIMILAR MEASURES ON MODELNET40.

Supervision	Layer	NN	FT	ST	F_measure	DCG	ANMRR
Unsupervised	S_G	0.84	0.67	0.82	0.27	0.70	0.27
	S_P	0.83	0.66	0.81	0.25	0.69	0.28
	S_I	0.82	0.65	0.80	0.24	0.68	0.29
	S_M	0.83	0.66	0.81	0.26	0.69	0.28
	$S_G + S_P + S_I + S_M$	0.85	0.69	0.84	0.30	0.73	0.26
Supervised	S_G	0.87	0.78	0.88	0.31	0.81	0.17
	S_P	0.89	0.80	0.90	0.32	0.83	0.15
	S_I	0.88	0.80	0.90	0.31	0.82	0.16
	S_M	0.90	0.81	0.91	0.33	0.84	0.15
	$S_G + S_P + S_I + S_M$	0.92	0.83	0.93	0.35	0.86	0.13

TABLE VII
PERFORMANCE ON DIFFERENT NUMBERS OF GEOMETRIC WORD ENTITIES ON MODELNET40.

Supervision	Number Words	NN	FT	ST	F_measure	DCG	ANMRR
Unsupervised	64	0.76	0.60	0.75	0.22	0.63	0.34
	128	0.79	0.62	0.76	0.24	0.65	0.31
	256	0.81	0.64	0.79	0.26	0.68	0.29
	512	0.83	0.67	0.81	0.28	0.70	0.27
	1024	0.85	0.69	0.84	0.30	0.73	0.26
	2048	0.84	0.67	0.82	0.28	0.71	0.27
Supervised	64	0.84	0.73	0.83	0.26	0.76	0.21
	128	0.86	0.77	0.87	0.30	0.80	0.17
	256	0.89	0.80	0.89	0.32	0.83	0.15
	512	0.90	0.81	0.91	0.33	0.84	0.14
	1024	0.92	0.83	0.93	0.35	0.86	0.13
	2048	0.91	0.82	0.91	0.33	0.84	0.13

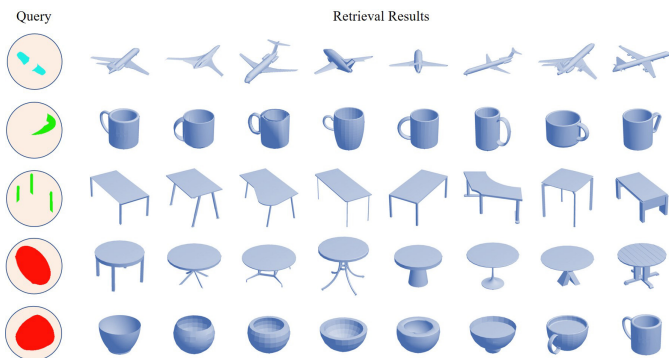


Fig. 8. Partial 3D model retrieval samples. (Zoom in for more details.)

the experimental outcomes, we discern a trend of improved retrieval results as the number of geometric words increases. Interestingly, we note that the optimal outcome is achieved when the number of geometric words reaches 1024, after which a gradual degradation in performance is observed.

This behavior can be attributed to the introduction of additional geometric words resulting in a sparser structural information landscape. As the number of geometric words grows, there is a possibility of similar parts from different virtual views of a 3D shape being mapped to distinct geometric words. Consequently, the coherence between the two models diminishes, causing the 3D shape knowledge graph to devolve into disjoint clusters. This phenomenon hampers the identification of analogous structural nodes and weakens the impact

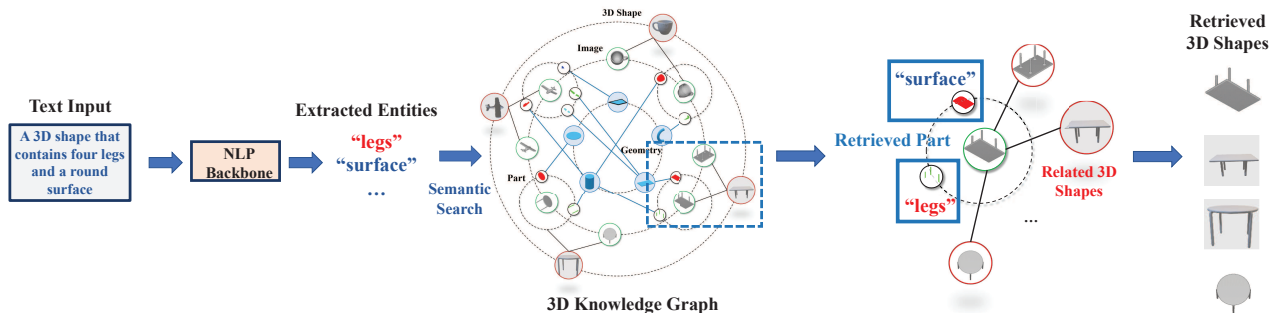


Fig. 9. Text-3D model retrieval framework.

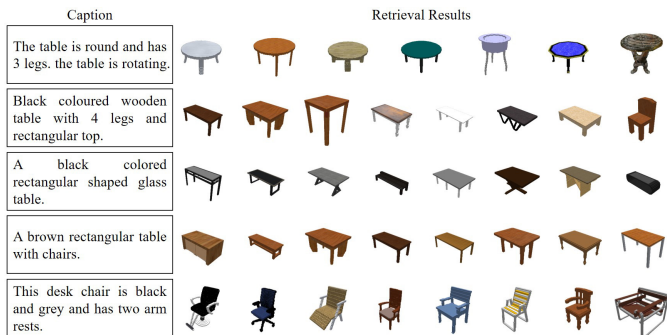


Fig. 10. Text-3D model retrieval samples.(Zoom in for more details.)

of the graph embedding process. In essence, the structural relationship information within the 3D shape knowledge graph becomes muddled with a smaller number of geometric words. Conversely, a larger number can lead to the convergence of various part structures onto the same geometric word, thereby diluting the structural information and negatively impacting embedding and retrieval performance.

H. Computational complexity

In this experiment, we conducted a comparison of the computational complexity of our model with that of several classic 3D representation methods, using the ModelNet40 dataset as a benchmark. We adopted DGCNN [61] as the reference method for this comparison. The comparison approaches have been selected based on their well-established recognition within the field. These approaches serve as essential benchmarks to establish a foundation for evaluating computational efficiency. The results in Table VIII presents a comparison of various methods in terms of their computational complexity for 3D shape analysis. Two important aspects are considered: model size and inference time.

Model Size: Smaller model sizes are generally desirable as they require less storage and memory. In this context, Pointnet has the smallest model size of 9.4 MB, followed closely by MVCNN with 11 MB. DGCNN and RotationNet have moderate model sizes of 21 MB and 36 MB, respectively. On the other hand, PointNet++ and PCNN have larger model

sizes of 12 MB and 94 MB, respectively. The proposed method has a model size of 51 MB.

Inference Time: Faster inference times are preferred as they lead to quicker predictions. Pointnet demonstrates the lowest inference time of 6.8 ms, followed by MVCNN with 12.3 ms. DGCNN and our method achieve inference times of 27.2 ms and 34 ms, respectively. The other methods, including RotationNet, PointNet++, and PCNN have longer inference times ranging from 117 ms to 163.2 ms.

Overall, the results indicate that our method performs competitively in terms of both model size and inference time compared to the other methods evaluated. We utilized the GCN model to generate node embeddings for retrieval purposes. Our GCN structure comprises only 3 layers, offering distinct advantages in terms of algorithm complexity when compared to traditional deep learning networks. It strikes a balance between model size and inference speed, showcasing promising computational efficiency. While Pointnet and MVCNN exhibit lower inference times, our method demonstrates a reasonable trade-off between model size and inference speed, positioning it as a viable option for efficient 3D shape analysis and recognition.

TABLE VIII
EXPERIMENTAL RESULTS FOR THE COMPUTATIONAL COMPLEXITY, WE REPORT THE MODEL SIZE AND INFERENCE TIME.

Method	Model Size (MB)	Inference Time (ms)
Pointnet[6]	9.4	6.8
PointNet++[13]	12	163.2
PCNN[77]	94	117
DGCNN[16]	21	27.2
MVCNN[3]	11	12.3
RotationNet[78]	36	121
Ours	51	34

V. EXTENDED APPLICATIONS BASED ON KNOWLEDGE GRAPH

This paper capitalizes on shape parts to generate geometric words, a pivotal component of our approach. These geometric words serve as building blocks for constructing the 3D shape knowledge graph and facilitating cross-domain 3D model retrieval. Our proposed knowledge graph is versatile, extending beyond its primary applications. In this section, we conduct

novel experiments to corroborate the effectiveness of the 3D shape knowledge graph in diverse contexts.

A. Partial 3D Shape Retrieval

The challenge here entails querying with incomplete 3D models. A partial 3D model retrieval system is tasked with returning a ranked list of complete models from a database based on their similarity to the query. Addressing this, we introduce an effective framework, as illustrated in Figure 7. The process involves extracting rendered images from the partial 3D model, followed by feature vector extraction using the ResNet-34 model [79]. These features facilitate the identification of analogous part entities within the 3D knowledge graph. Subsequently, we leverage this information to retrieve the relevant 3D shape based on these part entities. Figure 8 illustrates retrieval examples, substantiating the feasibility of our method.

B. Text-3D Shape Retrieval

The versatility of the 3D shape knowledge graph extends to text-to-shape retrieval scenarios. For instance, consider the query: "A 3D shape that features four legs and a rounded surface." We initiate the process by employing an NLP method [80] to extract entities from the given text. These entities are subsequently mapped to corresponding geometric shapes, which are further linked to geometric words or part entities within the 3D knowledge graph. The final step involves selecting 3D shapes with distinct relationships to these geometric words and part entities as the retrieval results. The conceptual framework is depicted in Figure 9, with retrieval instances showcased in Figure 10. We validate this concept using samples from the Text2Shape dataset [81], where the construction of the 3D shape knowledge graph and the mapping between geometric shapes and descriptions underscore the practical viability of our approach.

VI. CONCLUSION

This study introduces the innovative concept of the "geometric word," a foundational element within our 3D shape knowledge graph. Empirical results underscore the graph's efficacy in capturing and quantifying shape similarities. The "geometric word" concept bridges the gap between 3D shapes across different domains and the interface between 3D shapes and 2D images across varied modalities. Augmenting this notion, our graph embedding strategy harnesses graph structural information and effective similarity measures, making our approach a versatile tool for tackling challenges encompassing 3D shape retrieval and cross-domain 3D shape retrieval.

The empirical findings emphasize the significance of constructing knowledge graphs within the constraints of available data. Furthermore, the adaptability of "geometric words," learnable from a multitude of datasets, points toward the potential for a universal 3D shape knowledge graph akin to WordNet, capable of encompassing a broad spectrum of shape information. Future research will concentrate on realizing this universal 3D shape knowledge graph and exploring its applicability across diverse domains.

REFERENCES

- [1] Guo Y, Wang H, Hu Q, Liu H, Liu L, Bennamoun M. Deep learning for 3d point clouds: A survey. *IEEE transactions on pattern analysis and machine intelligence*. 2020;43(12):4338-64.
- [2] Wang N, Zhang Y, Li Z, Fu Y, Yu H, Liu W, et al. Pixel2Mesh: 3D mesh model generation via image guided deformation. *IEEE transactions on pattern analysis and machine intelligence*. 2020;43(10):3600-13.
- [3] Su H, Maji S, Kalogerakis E, Learned-Miller E. Multi-view convolutional neural networks for 3d shape recognition. In: *Proceedings of the IEEE international conference on computer vision*; 2015. p. 945-53.
- [4] Lei Y, Zhou Z, Zhang P, Guo Y, Ma Z, Liu L. Deep point-to-subspace metric learning for sketch-based 3D shape retrieval. *Pattern Recognit*. 2019;96.
- [5] Goldfeder C, Allen PK. Autotagging to improve text search for 3d models. In: *ACM/IEEE Joint Conference on Digital Libraries, JCDL 2008, Pittsburgh, PA, USA, June 16-20, 2008*; 2008. p. 355-8.
- [6] Qi CR, Su H, Mo K, Guibas LJ. Pointnet: Deep learning on point sets for 3d classification and segmentation. In: *Proceedings of the IEEE Conference on Computer Vision and Pattern Recognition*; 2017. p. 652-60.
- [7] Jiang J, Bao D, Chen Z, Zhao X, Gao Y. MLVCNN: Multi-loop-view convolutional neural network for 3D shape retrieval. In: *Proceedings of the AAAI conference on artificial intelligence*. vol. 33; 2019. p. 8513-20.
- [8] You H, Feng Y, Ji R, Gao Y. Pvnnet: A joint convolutional network of point cloud and multi-view for 3d shape recognition. In: *2018 ACM Multimedia Conference on Multimedia Conference*. ACM; 2018. p. 1310-8.
- [9] Dai G, Xie J, Fang Y. Deep Correlated Holistic Metric Learning for Sketch-Based 3D Shape Retrieval. *IEEE Transactions on Image Processing A Publication of the IEEE Signal Processing Society*. 2018;27(7):3374.
- [10] Long M, Wang J, Ding G, Sun J, Yu PS. Transfer joint matching for unsupervised domain adaptation. In: *Proceedings of the IEEE conference on computer vision and pattern recognition*; 2014. p. 1410-7.
- [11] Zhang J, Li W, Ogunbona P. Joint geometrical and statistical alignment for visual domain adaptation. In: *Proceedings of the IEEE conference on computer vision and pattern recognition*; 2017. p. 1859-67.
- [12] Wu Z, Song S, Khosla A, Yu F, Zhang L, Tang X, et al. 3d shapenets: A deep representation for volumetric shapes. In: *Proceedings of the IEEE conference on computer vision and pattern recognition*; 2015. p. 1912-20.
- [13] Qi CR, Yi L, Su H, Guibas LJ. Pointnet++: Deep hierarchical feature learning on point sets in a metric space. In: *Advances in neural information processing systems*; 2017. p. 5099-108.
- [14] Garro V, Giachetti A. Scale Space Graph Representation and Kernel Matching for Non Rigid and Textured 3D Shape Retrieval. *IEEE Trans Pattern Anal Mach Intell*. 2016;38(6):1258-71.

- [15] Xie J, Dai G, Zhu F, Wong EK, Fang Y. DeepShape: Deep-Learned Shape Descriptor for 3D Shape Retrieval. *IEEE Trans Pattern Anal Mach Intell.* 2017;39(7):1335-45.
- [16] Wang Y, Sun Y, Liu Z, Sarma SE, Bronstein MM, Solomon JM. Dynamic graph cnn for learning on point clouds. *ACM Transactions on Graphics (tog).* 2019;38(5):1-12.
- [17] Chen DY, Tian XP, Shen YT, Ming O. On Visual Similarity Based 3D Model Retrieval. *Computer Graphics Forum.* 2010;22(3):223-32.
- [18] Bai S, Bai X, Zhou Z, Zhang Z, Tian Q, Latecki LJ. GIFT: Towards Scalable 3D Shape Retrieval. *IEEE Transactions on Multimedia.* 2017 June;19(6):1257-71.
- [19] Sfikas K, Pratikakis I, Theoharis T. Ensemble of panorama-based convolutional neural networks for 3d model classification and retrieval. *Computers & Graphics.* 2018;71:208-18.
- [20] Wang C, Samari B, Siddiqi K. Local Spectral Graph Convolution for Point Set Feature Learning. In: *Computer Vision - ECCV 2018 - 15th European Conference, Munich, Germany, September 8-14, 2018, Proceedings, Part IV.* vol. 11208 of *Lecture Notes in Computer Science.* Springer; 2018. p. 56-71.
- [21] Te G, Hu W, Zheng A, Guo Z. Rgcnn: Regularized graph cnn for point cloud segmentation. In: *Proceedings of the 26th ACM international conference on Multimedia;* 2018. p. 746-54.
- [22] Shi W, Rajkumar R. Point-GNN: Graph Neural Network for 3D Object Detection in a Point Cloud. In: *2020 IEEE/CVF Conference on Computer Vision and Pattern Recognition, CVPR 2020, Seattle, WA, USA, June 13-19, 2020.* IEEE; 2020. p. 1708-16.
- [23] Zhang C, Yu J, Song Y, Cai W. Exploiting edge-oriented reasoning for 3d point-based scene graph analysis. In: *Proceedings of the IEEE/CVF conference on computer vision and pattern recognition;* 2021. p. 9705-15.
- [24] Zhang L, Chang X, Liu J, Luo M, Li Z, Yao L, et al. Tn-zstad: Transferable network for zero-shot temporal activity detection. *IEEE Transactions on Pattern Analysis and Machine Intelligence.* 2022;45(3):3848-61.
- [25] Li Z, Xu P, Chang X, Yang L, Zhang Y, Yao L, et al. When object detection meets knowledge distillation: A survey. *IEEE Transactions on Pattern Analysis and Machine Intelligence.* 2023.
- [26] Li M, Huang PY, Chang X, Hu J, Yang Y, Hauptmann A. Video pivoting unsupervised multi-modal machine translation. *IEEE Transactions on Pattern Analysis and Machine Intelligence.* 2022;45(3):3918-32.
- [27] He S, Wang W, Wang Z, Xu X, Yang Y, Wang X, et al. Category alignment adversarial learning for cross-modal retrieval. *IEEE Transactions on Knowledge and Data Engineering.* 2022;35(5):4527-38.
- [28] Li Z, Tang J, Mei T. Deep collaborative embedding for social image understanding. *IEEE transactions on pattern analysis and machine intelligence.* 2018;41(9):2070-83.
- [29] Li Z, Tang J. Weakly supervised deep metric learning for community-contributed image retrieval. *IEEE Transactions on Multimedia.* 2015;17(11):1989-99.
- [30] Mu P, Zhang S, Zhang Y, Ye X, Pan X. Image-based 3D model retrieval using manifold learning. *Journal of Zhejiang University Science C.* 2018;19(11):1397-408.
- [31] Li Y, Su H, Qi CR, Fish N, Cohenor D, Guibas LJ. Joint embeddings of shapes and images via CNN image purification. *international conference on computer graphics and interactive techniques.* 2015;34(6):234.
- [32] Han Z, Shang M, Liu Z, Vong CM, Liu Y, Zwicker M, et al. SeqViews2SeqLabels: Learning 3D Global Features via Aggregating Sequential Views by RNN With Attention. *IEEE Transactions on Image Processing.* 2019;28(2):658-72.
- [33] Nie W, Wang Y, Song D, Li W. 3D Model Retrieval Based on a 3D Shape Knowledge Graph. *IEEE Access.* 2020;8:142632-41.
- [34] Liu Z, Freeman WT, Tenenbaum JB, Wu J. Physical primitive decomposition. In: *Proceedings of the European Conference on Computer Vision (ECCV);* 2018. p. 3-19.
- [35] Katageri S, Kulmi S, Tabib RA, Mudenagudi U. PointD-CCNet: 3D Object Categorization Network Using Point Cloud Decomposition. In: *Proceedings of the IEEE/CVF Conference on Computer Vision and Pattern Recognition;* 2021. p. 2200-8.
- [36] Ahmed A, Jalal A, Kim K. RGB-D images for object segmentation, localization and recognition in indoor scenes using feature descriptor and Hough voting. In: *2020 17th International Bhurban Conference on Applied Sciences and Technology (IBCAST).* IEEE; 2020. p. 290-5.
- [37] Zhuang C, Wang Z, Zhao H, Ding H. Semantic part segmentation method based 3D object pose estimation with RGB-D images for bin-picking. *Robotics and Computer-Integrated Manufacturing.* 2021;68:102086.
- [38] Wang J, Xu C, Dai L, Zhang J, Zhong RY. An Unequal Learning Approach for 3D Point Cloud Segmentation. *IEEE Transactions on Industrial Informatics.* 2020.
- [39] Feng Y, Zhang Z, Zhao X, Ji R, Gao Y. GVCNN: Group-view convolutional neural networks for 3D shape recognition. In: *Proceedings of the IEEE Conference on Computer Vision and Pattern Recognition;* 2018. p. 264-72.
- [40] Mo K, Zhu S, Chang AX, Yi L, Tripathi S, Guibas LJ, et al. Partnet: A large-scale benchmark for fine-grained and hierarchical part-level 3d object understanding. In: *Proceedings of the IEEE/CVF Conference on Computer Vision and Pattern Recognition;* 2019. p. 909-18.
- [41] Yi L, Guibas L, Hertzmann A, Kim VG, Su H, Yumer E. Learning hierarchical shape segmentation and labeling from online repositories. *arXiv preprint arXiv:170501661.* 2017.
- [42] Yu F, Liu K, Zhang Y, Zhu C, Xu K. Partnet: A recursive part decomposition network for fine-grained and hierarchical shape segmentation. In: *Proceedings of the IEEE/CVF Conference on Computer Vision and Pattern Recognition;* 2019. p. 9491-500.
- [43] Kalogerakis E, Averkiou M, Maji S, Chaudhuri S. 3D shape segmentation with projective convolutional net-

- works. In: proceedings of the IEEE conference on computer vision and pattern recognition; 2017. p. 3779-88.
- [44] Li Z, Sun Y, Zhang L, Tang J. CTNet: Context-based tandem network for semantic segmentation. *IEEE Transactions on Pattern Analysis and Machine Intelligence*. 2021;44(12):9904-17.
- [45] Burgess CP, Matthey L, Watters N, Kabra R, Higgins I, Botvinick M, et al. Monet: Unsupervised scene decomposition and representation. *arXiv preprint arXiv:190111390*. 2019.
- [46] Nguyen-Phuoc T, Li C, Theis L, Richardt C, Yang YL. Hologan: Unsupervised learning of 3d representations from natural images. In: *Proceedings of the IEEE/CVF International Conference on Computer Vision*; 2019. p. 7588-97.
- [47] Ronneberger O, Fischer P, Brox T. U-Net: Convolutional Networks for Biomedical Image Segmentation. In: *Medical Image Computing and Computer-Assisted Intervention – MICCAI 2015*. Cham: Springer International Publishing; 2015. p. 234-41.
- [48] Badrinarayanan V, Kendall A, Cipolla R. SegNet: A Deep Convolutional Encoder-Decoder Architecture for Image Segmentation. *IEEE Transactions on Pattern Analysis Machine Intelligence*. 2017:1-1.
- [49] Zhao H, Shi J, Qi X, Wang X, Jia J. Pyramid scene parsing network. In: *Proceedings of the IEEE conference on computer vision and pattern recognition*; 2017. p. 2881-90.
- [50] Chen LC, Papandreou G, Schroff F, Adam H. Rethinking atrous convolution for semantic image segmentation. *arXiv preprint arXiv:170605587*. 2017.
- [51] Wold S, Esbensen K, Geladi P. Principal component analysis. *Chemometrics and intelligent laboratory systems*. 1987;2(1-3):37-52.
- [52] Papadakis P, Pratikakis I, Perantonis S, Theoharis T. Efficient 3D shape matching and retrieval using a concrete radialized spherical projection representation. *Pattern Recognition*. 2007;40(9):2437-2452.
- [53] Wang W, Zhao S, Shen J, Hoi SC, Borji A. Salient object detection with pyramid attention and salient edges. In: *Proceedings of the IEEE Conference on Computer Vision and Pattern Recognition*; 2019. p. 1448-57.
- [54] He K, Zhang X, Ren S, Sun J. Identity mappings in deep residual networks. In: *European conference on computer vision*. Springer; 2016. p. 630-45.
- [55] Hamilton W, Ying Z, Leskovec J. Inductive representation learning on large graphs. In: *Advances in neural information processing systems*; 2017. p. 1024-34.
- [56] Gao Y, Dai Q, Wang M, Zhang N. 3D model retrieval using weighted bipartite graph matching. *Signal Processing: Image Communication*. 2011;26(1):39-47.
- [57] Li W, Liu A, Nie W, Song D, Li Y, Wang W, et al. Monocular Image Based 3D Model Retrieval. In: *12th Eurographics Workshop on 3D Object Retrieval, 3DORS*. Eurographics Association; 2019. p. 103-10.
- [58] Liu AA, Nie WZ, Gao Y, Su YT. View-based 3-D model retrieval: a benchmark. *IEEE transactions on cybernetics*. 2017;48(3):916-28.
- [59] Kazhdan M, Funkhouser T, Rusinkiewicz S. Rotation invariant spherical harmonic representation of 3 d shape descriptors. In: *Symposium on geometry processing*. vol. 6; 2003. p. 156-64.
- [60] Qi CR, Su H, Nießner M, Dai A, Yan M, Guibas LJ. Volumetric and multi-view cnns for object classification on 3d data. In: *Proceedings of the IEEE conference on computer vision and pattern recognition*; 2016. p. 5648-56.
- [61] Wang Y, Sun Y, Liu Z, Sarma SE, Bronstein MM, Solomon JM. Dynamic graph cnn for learning on point clouds. *arXiv preprint arXiv:180107829*. 2018.
- [62] Chen DY, Tian XP, Shen YT, Ouhyoung M. On visual similarity based 3D model retrieval. In: *Computer graphics forum*. vol. 22. Wiley Online Library; 2003. p. 223-32.
- [63] Allen M, Girod L, Newton R, Madden S, Blumstein DT, Estrin D. Voxnet: An interactive, rapidly-deployable acoustic monitoring platform. In: *2008 International Conference on Information Processing in Sensor Networks (ipsn 2008)*. IEEE; 2008. p. 371-82.
- [64] Brock A, Lim T, Ritchie JM, Weston N. Generative and Discriminative Voxel Modeling with Convolutional Neural Networks. *Computer Science*. 2016.
- [65] Yu Q, Yang C, Fan H, Wei H. Latent-MVCNN: 3D shape recognition using multiple views from pre-defined or random viewpoints. *Neural Processing Letters*. 2020;52:581-602.
- [66] Ma Y, Zheng B, Guo Y, Lei Y, Zhang J. Boosting multi-view convolutional neural networks for 3d object recognition via view saliency. In: *Chinese Conference on Image and Graphics Technologies*. Springer; 2017. p. 199-209.
- [67] He X, Huang T, Bai S, Bai X. View n-gram network for 3D object retrieval. In: *Proceedings of the IEEE International Conference on Computer Vision*; 2019. p. 7515-24.
- [68] Guo MH, Cai JX, Liu ZN, Mu TJ, Martin RR, Hu SM. Pct: Point cloud transformer. *Computational Visual Media*. 2021;7:187-99.
- [69] Gao Z, Zhang Y, Zhang H, Guan W, Feng D, Chen S. Multi-level view associative convolution network for view-based 3D model retrieval. *IEEE Transactions on Circuits and Systems for Video Technology*. 2021;32(4):2264-78.
- [70] Ganin Y, Lempitsky VS. Unsupervised Domain Adaptation by Backpropagation. In: *Proceedings of the 32nd International Conference on Machine Learning, ICML 2015, Lille, France, 6-11 July 2015*. vol. 37 of *JMLR Workshop and Conference Proceedings*. JMLR.org; 2015. p. 1180-9.
- [71] Long M, Zhu H, Wang J, Jordan MI. Deep Transfer Learning with Joint Adaptation Networks. In: *Proceedings of the 34th International Conference on Machine Learning, ICML 2017, Sydney, NSW, Australia, 6-11 August 2017*. vol. 70 of *Proceedings of Machine Learning Research*. PMLR; 2017. p. 2208-17.

- [72] Zhang J, Li W, Ogunbona P. Joint Geometrical and Statistical Alignment for Visual Domain Adaptation. In: 2017 IEEE Conference on Computer Vision and Pattern Recognition, CVPR 2017, Honolulu, HI, USA, July 21-26, 2017. IEEE Computer Society; 2017. p. 5150-8.
- [73] Long M, Wang J, Ding G, Sun J, Yu PS. Transfer feature learning with joint distribution adaptation. In: Proceedings of the IEEE international conference on computer vision; 2013. p. 2200-7.
- [74] Song D, Zhang CM, Zhao XQ, Wang T, Nie WZ, Li XY, et al. Self-supervised image-based 3d model retrieval. *ACM Transactions on Multimedia Computing, Communications and Applications*. 2023;19(2):1-18.
- [75] Li W, Zhang Y, Wang F, Li X, Duan Y, Liu AA. Instance-prototype similarity consistency for unsupervised 2D image-based 3D model retrieval. *Information Processing & Management*. 2023;60(4):103372.
- [76] Wang J, Feng W, Chen Y, Yu H, Huang M, Yu PS. Visual domain adaptation with manifold embedded distribution alignment. In: Proceedings of the 26th ACM international conference on Multimedia; 2018. p. 402-10.
- [77] Li Y, Bu R, Sun M, Wu W, Di X, Chen B. Pointcnn: Convolution on x-transformed points. *Advances in neural information processing systems*. 2018;31.
- [78] Kanezaki A, Matsushita Y, Nishida Y. Rotationnet: Joint object categorization and pose estimation using multi-views from unsupervised viewpoints. In: Proceedings of the IEEE Conference on Computer Vision and Pattern Recognition; 2018. p. 5010-9.
- [79] He K, Zhang X, Ren S, Sun J. Deep Residual Learning for Image Recognition. In: 2016 IEEE Conference on Computer Vision and Pattern Recognition, CVPR 2016, Las Vegas, NV, USA, June 27-30, 2016. IEEE Computer Society; 2016. p. 770-8.
- [80] Peng Y, Chi J. Unsupervised Cross-Media Retrieval Using Domain Adaptation With Scene Graph. *IEEE Trans Circuits Syst Video Technol*. 2020;30(11):4368-79.
- [81] Chen K, Choy CB, Savva M, Chang AX, Funkhouser T, Savarese S. Text2shape: Generating shapes from natural language by learning joint embeddings. In: Asian Conference on Computer Vision. Springer; 2018. p. 100-16.